

Elastic and breaking properties of epitaxial face-centered crystals in neutron star crusts and white dwarf cores

D. A. Baiko^{*}

Ioffe Institute, Politekhnikeskaya 26, 194021 Saint Petersburg, Russia

Accepted; Received ; in original form

ABSTRACT

Crystallization of dense matter in neutron star crusts and white dwarf cores may be similar to epitaxial crystal growth in terrestrial laboratories. However in stellar crystals, the spacing between horizontal planes has to gradually increase with the outward movement of the crystallization front, tracing decrease of the electron density. This process produces Coulomb crystals with stretched rather than cubic elementary cells. We extend the analysis of the elastic and breaking properties of such crystals to the face-centered (fc) lattice. Shear deformations orthogonal to the stretch direction have been studied for 22 crystallographic shear planes. A common property for all these planes is a reduction and eventual nulling of the breaking shear strain with deviation from the unstretched configuration. The effective shear moduli for deformations orthogonal to the stretch direction have been calculated. It is possible that the epitaxial crystallization in compact stars results in a formation of large-scale crystallites or, at least, in growth of the whole crystallization front perpendicular to particular crystallographic planes. For fc structure growth orthogonal to the {111} planes, we expect that, at any density, $\sim 5\%$ ($\sim 0.5\%$) of crystallite height is occupied by layers one (two) orders of magnitude weaker than the bulk of the crystallite. This may be important for realistic modeling of crustquakes on neutron stars.

Key words: dense matter – equation of state – stars: neutron – white dwarfs.

1 INTRODUCTION

Some of the best known works of Kenneth Golden and Gabor Kalman (Carini, Kalman & Golden 1982; Kalman & Golden 1990; Golden, Kalman & Wynn 1992; Golden & Kalman 2000; Donkó, Kalman & Golden 2002) have been devoted to theoretical studies of one-component plasma (OCP). The OCP is a system of identical point charges (hereafter ions) immersed into incompressible uniform charge-neutralizing background (hereafter electrons). This system is of fundamental importance for plasma physics and condensed matter physics as one of the simplest models in which effects of strong non-ideality of ions as well as ion quantum effects can be studied by various theoretical methods. The OCP is also highly relevant for astrophysics of compact stars, white dwarfs (WD) and neutron stars (NS) (e.g. Haensel, Potekhin & Yakovlev 2007). In these objects, under the action of enormous gravity, matter is compressed to extremely high densities (up to $\sim 10^{10}$ g/cc for WD and $\sim 10^{14}$ g/cc for NS crust) which are practically unreachable in Earth laboratories. At such densities, atoms are fully ionized whereas electrons are strongly degenerate.

Electrons form the charge-neutralizing background which, in many problems, can be treated as constant and uniform (e.g. Haensel et al. 2007).

One of the more interesting features of the OCP in the compact stars is its inevitable crystallization in the course of stellar cooling (e.g. Van Horn 1968). The main difference between crystallized and liquid forms of the OCP is the property of the former to support finite stretch and shear deformations, to yield if a critical deformation is exceeded, and to possess a spectrum of transverse acoustic phonon modes related to these phenomena. Long-lived shear eigenmodes are also known in the liquid OCP under conditions of strong coupling (Hansen, McDonald & Pollock 1975; Golden et al. 1992). There is an intimate connection between eigenmodes of the liquid OCP and phonon modes in its crystallized state (e.g. Golden et al. 1992; Ott et al. 2013).

Elastic and breaking properties of the crystallized OCP are very important for astrophysics of compact stars. First of all, they are crucial for theoretical studies of magnetars, NS with extremely strong magnetic field, in excess of $\sim 10^{14}$ G. In these objects, elastic and breaking properties of NS crust are used for building models of crustquakes and for an analysis of spectra of quasi-periodic oscillations observed in hyperflares and associated with torsional vibrations of the

^{*} E-mail: baiko@astro.ioffe.ru

crust (e.g. Kaspi & Beloborodov 2017). Breaking strain of NS crust also determines maximum height of “mountains” which the crust can support. The mountains, in turn, determine the mass quadrupole of a NS, a non-zero value of which is necessary for a rotating NS to emit gravitational waves (Ushomirsky, Cutler & Bildsten 2000).

It is long established that the crystallization front in compact stars moves from the deeper layers up, towards the surface (e.g. Van Horn 1968). This is connected with the fact that the thermal conductivity of degenerate electrons is very high and the stellar temperature has a less steep profile than that of the crystallization temperature. Crystallization in these stars is a near-equilibrium process which takes billions of years to complete in WD and hundreds-to-thousands years in NS crust. The outcome of such near-equilibrium bottom-up crystallization of dense matter has been revisited in a recent paper (Baiko 2024, hereafter Paper I). In this work, it has been argued that already formed crystal layers create above themselves an ordered two-dimensional relief of electrostatic potential. The scale of variations of the potential (e.g. potential well depth) is significantly greater than typical ion kinetic energies at crystallization. The lateral extent of the wells is comparable with the lattice spacing, so that newly crystallizing ions can be easily captured by them. There is no dependence on orientation of impinging ions (as would be the case for covalent bonds). Vertical positions of the potential minima with respect to the last crystallized surface are controlled by the density of electrons. All these properties tend to facilitate two-dimensional nucleation of new crystal layers on top of the previous ones as opposed to three-dimensional nucleation of new crystallites (made of repulsing atomic nuclei) in the midst of the liquid. In semiconductor physics and industry, such crystal growth from a liquid which preserves the microscopic order of a seed is known as the liquid-phase epitaxy (see Paper I for an extensive list of references).

Epitaxial crystal growth preserves the ion surface density, σ . From charge neutrality, $\sigma = \eta n_e / Z$, where η is the interplane spacing in the vertical direction, n_e is the electron density, and Z is the ion charge number. Consequently, the epitaxial growth is accompanied by gradual vertical stretching (more precisely, elongation) of crystal elementary cells in response to pressure and electron density reduction as the crystallization front moves outward (Paper I). In other words, η gradually increases while horizontal ion spacings remain constant. We characterize the amount of stretch by the stretch factor, ξ . The stretch factor is the ratio of vertical to horizontal lattice scales which would be equal to 1 in an unstretched lattice. Elongation corresponds to $\xi > 1$. Growth of contracted crystals ($\xi < 1$) is also possible if the front moves across a (relatively thin) layer where the average ion charge number $\langle Z \rangle$ decreases with decrease of depth (at approximately constant n_e) under the assumption that a regular lattice still forms throughout (Paper I). Finally, it is known that overstretched crystals develop unstable phonon modes and break, which limits the vertical sizes of growing crystallites (Baiko & Kozhberov 2017; Baiko & Chugunov 2018).

2 METHODS

2.1 General remarks

In this paper, we aim to extend the results of Paper I from body-centered cubic (bcc) to face-centered cubic (fcc) crystals. Let us note that, taking into account the possibility of crystal stretching, it will be more accurate in some contexts to speak about general face-centered (fc) or body-centered (bc) lattices. In terrestrial experiments on crystal growth, the fcc lattice occurs much more often than the bcc one with growth perpendicular to $\{111\}$ planes particularly prominent. On the contrary, in the literature on compact stars, the bcc lattice is more popular due to its advantage over any other lattice in terms of the potential (Madelung) energy for the OCP of bare atomic nuclei on the constant and uniform neutralizing background. However, the difference between bcc and fcc energies for unstretched material is tiny, and once the possibility of crystal stretch is allowed, the preference for a bc lattice becomes even less solidly justified.

We shall begin by calculating breaking strain for shear deformations perpendicular to a crystal stretch direction. As mentioned in Paper I, such statement of the problem is relevant for astrophysics of compact stars in which stretch is aligned with gravity whereas horizontal shear can be due to weaker forces (e.g. magnetic) which do not perturb the hydrostatic equilibrium. Since a crystal can be oriented differently and thus stretched in different crystallographic directions, this may involve shear in different crystallographic planes. Within each plane, any azimuthal angle of the shear is possible.

In the *polycrystalline* picture of stellar matter described in Paper I, namely, if, at any given depth, there exist randomly oriented crystallites stretched vertically by the same factor ξ , we expect breaking of matter to be associated with the crystallite with the minimum breaking shear strain. To find the latter, at each ξ and for each plane, we minimize the breaking strain over the azimuthal angle and then minimize over the planes. In Paper I, for the bc lattice, we have performed minimization over 3 high-symmetry planes and 4 auxiliary, less symmetric planes. For this work on the fc lattice, we have significantly expanded the set of considered configurations and have studied shear deformations in all crystallographic planes with Miller indices ≤ 4 . There are 22 such planes, which are listed in Table 1.

2.2 Lattice geometry

Let us specify a cartesian reference frame whose axes are aligned with the fcc lattice cube (before stretch) and one of the ions is taken as the origin. The shear planes which we consider, have intercepts with x , y , and z -axes denoted as a , b , and c , respectively. Based on lattice symmetry, we require that, if two of the intercepts are at infinity, then $a > 0$ is finite. This is the case of crystal growth perpendicular to a $\{100\}$ plane. If only one of the intercepts is at infinity, then a and b are finite, $a \geq b > 0$, and the equality corresponds to growth perpendicular to a $\{110\}$ plane. If all intercepts are finite, then either $a > b > c > 0$ or $a = b > 0$ whereas $c > 0$ can be less, greater, or equal to $a = b$. The case, where all three intercepts are equal, corresponds to the crystal growth perpendicular to a $\{111\}$ plane.

Let us define basis vectors of a new cartesian reference frame by their coordinates in the original basis as $\mathbf{e}_1 = (-a, b, 0)/\sqrt{s_2}$, $\mathbf{e}_2 = (-ab^2, -a^2b, cs_2)/\sqrt{s_2s_4}$, and $\mathbf{e}_3 = (bc, ca, ab)/\sqrt{s_4}$, where $s_2 = a^2 + b^2$ and $s_4 = a^2b^2 + b^2c^2 + c^2a^2$. If $c \rightarrow \infty$, $\mathbf{e}_2 \rightarrow (0, 0, 1)$ and $\mathbf{e}_3 \rightarrow (b, a, 0)/\sqrt{s_2}$. If also $b \rightarrow \infty$, then $\mathbf{e}_1 \rightarrow (0, 1, 0)$ and, further, $\mathbf{e}_3 \rightarrow (1, 0, 0)$. In all cases, vector \mathbf{e}_3 coincides with the stretch direction, whereas vectors \mathbf{e}_1 and \mathbf{e}_2 belong to the plane of the shear.

The stretched fc lattice basis vectors and the respective reciprocal lattice basis vectors in the basis $(\mathbf{e}_1, \mathbf{e}_2, \mathbf{e}_3)$ are given in Table 1 for 22 variants of the shear plane. For non-deformed fcc lattice, one has to set $\xi = 1$ and $\theta_1 = \theta_2 = 0$ in these expressions. To find the breaking shear strain, we stretch and then shear the crystal, which is accomplished by a modification of the third lattice basis vector: its \mathbf{e}_3 -component is multiplied by ξ for stretch, and then, for shear, its in-plane components are augmented by $\theta_1 = \theta \cos \chi$ and $\theta_2 = \theta \sin \chi$. In this case, θ is the amplitude of the shear and χ is its azimuthal angle.

2.3 Unstable phonon modes

Given direct and reciprocal vectors of a deformed lattice, one can construct its dynamic matrix which yields frequencies of the lattice eigenmodes (phonons). An initially stable lattice loses stability under a large enough deformation which is signified by the appearance of a phonon mode with a negative squared frequency at some wave vector. In the problem of Coulomb crystal breaking under an excessive stretch or shear deformation, the unstable mode first appears at the Brillouin zone center. Near the center, the phonon frequencies are strongly dependent on the wave vector direction. Strictly speaking, at the center, the phonon frequencies are non-analytic. With deformation increase beyond the critical magnitude, the zone of unstable wave vectors rapidly widens over some finite range. Consequently, we approximate the critical deformation by the value which produces an unstable mode at a very small but finite wave vector.

We scanned a dense grid of non-equivalent spherical angles of a phonon wave vector assuming its length equal to $(1/50)2\pi/a_1$. For deformed fc lattices, a_1 is defined by $n_i a_1^3 \xi = 4$, where n_i is the ion density. Given a shear plane and χ , at each ξ , we looked for the maximum shear deformation of a stretched crystal, at which the dynamic matrix determinant remained positive. We then minimized these maximum deformations over a dense grid of χ .

3 RESULTS

3.1 Breaking shear strain of dense stretched matter

In order to represent the results, let us recall the standard strain tensor definition $u_{ij} = 0.5(\partial u_i / \partial r_j + \partial u_j / \partial r_i)$, where u_i is the displacement, which, in this problem, we shall evaluate with respect to the stretched configuration; i and j are cartesian indices. Let us define two cartesian axes, $\hat{\theta}$ and $\hat{\eta} = \mathbf{e}_3$, along the direction of the shear and along the direction of the stretch, respectively. The applied shear results in the appearance of non-zero components

$u_{\theta\eta} = u_{\eta\theta} \equiv \varepsilon/2 = \theta/(2\eta)$, where ε is the deformation parameter and η is the interplane spacing. The latter is equal to the \mathbf{e}_3 -component of the third lattice basis vector (cf. Table 1). We denote the maximum deformation parameter, at which the lattice is still stable, minimized over χ as $\varepsilon_{\text{crit}}$ and plot it in Fig. 1 as a function of ξ , separately for each crystallographic plane considered. In particular, we plot $\varepsilon_{\text{crit}}$ for crystals stretched perpendicular to crystallographic planes with the maximum Miller index equal to 1 or 2 (panel a), 3 (panel b), and 4 (panel c).

In all panels of Fig. 1, grey lines show the entire family of $\varepsilon_{\text{crit}}(\xi)$ curves for 22 considered planes. In panel 1a, thick (green), intermediate (red), and thin (blue) curves correspond to stretches orthogonal to $\{100\}$, $\{111\}$, and $\{110\}$ planes, respectively. Purple long-dashed, short-dashed, and dot-dashed curves correspond to stretches orthogonal to $\{210\}$, $\{211\}$, and $\{221\}$ planes, respectively. In panels 1b and c, coloured curves of various types display $\varepsilon_{\text{crit}}(\xi)$ for stretches orthogonal to planes with the maximum Miller index of 3 and 4, respectively, as detailed in the legends.

These results are very similar to those for the bc lattice obtained in Paper I. A common property for all¹ planes is a reduction of breaking shear strain with deviation of the stretch factor from 1 and especially with its approach to the breaking limit for stretch, ξ_{crit} , defined as $\varepsilon_{\text{crit}}(\xi_{\text{crit}}) = 0$. Shear deformations in different planes are characterized by significantly different breaking properties.

For the *polycrystalline* scenario, in panel 1d, red dots show minimized over 22 planes breaking shear strain. These data are given in the second column of Table 2 with Miller indices of a plane, realizing the minimum at a given ξ , reported in the third column. The minimized breaking shear strain can be fitted to rms fit accuracy better than 0.05% by a simple analytic expression:

$$\begin{aligned} \varepsilon_{\text{crit}}^{\min} &= 0.0546 - 20.2 (\xi^{2/3} - 1.0017)^2 \\ &\quad - 7.6\text{e}6 (\xi^{2/3} - 1.0036)^6. \end{aligned} \quad (1)$$

For comparison, dot-dashed (dark-green) curve demonstrates the analogous fit obtained in Paper I (equation 14) for stretched bc lattice. Just like in the case of the bc lattice, the $\varepsilon_{\text{crit}}^{\min}(\xi)$ curve is essentially parabolic.

For the unstretched fcc lattice, $\varepsilon_{\text{crit}}^{\min}(1) \approx 0.055$ (to be compared with ≈ 0.064 for bcc). Breaking stretch factor for the fc lattice is found as $\xi_{\text{crit}} \approx 0.95$ and 1.06 for contractions and elongations, respectively. Introducing stretch strain $\tilde{\varepsilon} \equiv \xi^{2/3} - 1$, we obtain, respectively, $\tilde{\varepsilon}_{\text{crit}} \approx -0.034$ and 0.04. This can be compared with $|\tilde{\varepsilon}_{\text{crit}}| \approx 0.04$ reported for the bc lattice by Baiko & Chugunov (2018) (in reasonable agreement with the dot-dashed curve in Fig. 1d).

In general, we see that the locus of breaking strain minima of the fc lattice lies systematically below that for the bc structure. We do not think that this is related to the fact that fewer stretch orientations have been analyzed in Paper I, because in both cases, for certain ξ , the minimum curve is bounded by critical curves for low-index planes.

The solid red curve in Fig. 1d, the same as in Fig. 1a,

¹ except for $\{100\}$ planes which can tolerate a very strong contraction from $\xi = 1$ to $\xi = 1/\sqrt{2}$, describing a structural transition from fcc to bcc lattice; see also Baiko & Kozhberov (2017) and Paper I

Table 1. Lattice parameters. Column 1 shows Miller indices of a shear plane and the number of equivalent planes. Columns 2 and 3 are coordinates of direct and reciprocal basis vectors, respectively, in the basis described in the text.

Miller index N_{eqv}	direct lattice basis (units $a_1/2$)	reciprocal lattice basis (units $2\pi/a_1$)
cube-diagonal, {111} 8	$(\sqrt{2}, 0, 0)$	$(\sqrt{2}, -\sqrt{2}/3, -(1/\sqrt{3} + \sqrt{3}/2 \theta_1 - \theta_2/\sqrt{2})/\xi)$
	$(1/\sqrt{2}, \sqrt{3}/2, 0)$	$(0, \sqrt{8}/3, -(1/\sqrt{3} + \sqrt{2}\theta_2)/\xi)$
	$(1/\sqrt{2} + \theta_1, 1/\sqrt{6} + \theta_2, \xi/\sqrt{4/3})$	$(0, 0, \sqrt{3}/\xi)$
cube-edge, {100} 6	$(2, 0, 0)$	$(1, -1, -(1 + \theta_1 - \theta_2)/\xi)$
	$(1, 1, 0)$	$(0, 2, -2\theta_2/\xi)$
	$(1 + \theta_1, \theta_2, \xi)$	$(0, 0, 2/\xi)$
face-diagonal, {110} 12	$(\sqrt{2}, 0, 0)$	$(\sqrt{2}, 0, -(\sqrt{2} + 2\theta_1)/\xi)$
	$(0, 2, 0)$	$(0, 1, -\sqrt{2}(1 + \theta_2)/\xi)$
	$(1/\sqrt{2} + \theta_1, 1 + \theta_2, \xi/\sqrt{2})$	$(0, 0, \sqrt{8}/\xi)$
{210} 24	$(\sqrt{20}, 0, 0)$	$(1/\sqrt{5}, -1, -(3/\sqrt{5} + \theta_1 - \sqrt{5}\theta_2)/\xi)$
	$(\sqrt{5}, 1, 0)$	$(0, 2, -\sqrt{20}\theta_2/\xi)$
	$(3/\sqrt{5} + \theta_1, \theta_2, \xi/\sqrt{5})$	$(0, 0, \sqrt{20}/\xi)$
{310} 24	$(\sqrt{10}, 0, 0)$	$(2/\sqrt{10}, 0, -(14/\sqrt{10} + 2\theta_1)/\xi)$
	$(0, 2, 0)$	$(0, 1, -\sqrt{10}(1 + \theta_2)/\xi)$
	$(7/\sqrt{10} + \theta_1, 1 + \theta_2, \xi/\sqrt{10})$	$(0, 0, \sqrt{40}/\xi)$
{320} 24	$(\sqrt{52}, 0, 0)$	$(1/\sqrt{13}, -1, -(5/\sqrt{13} + \theta_1 - \sqrt{13}\theta_2)/\xi)$
	$(\sqrt{13}, 1, 0)$	$(0, 2, -\sqrt{52}\theta_2/\xi)$
	$(5/\sqrt{13} + \theta_1, \theta_2, \xi/\sqrt{13})$	$(0, 0, \sqrt{52}/\xi)$
{211} 24	$(\sqrt{2}, 0, 0)$	$(\sqrt{2}, 0, -\sqrt{6}(1 + \sqrt{2}\theta_1)/\xi)$
	$(0, \sqrt{12}, 0)$	$(0, 1/\sqrt{3}, -\sqrt{2}(2/\sqrt{3} + \theta_2)/\xi)$
	$(1/\sqrt{2} + \theta_1, 2/\sqrt{3} + \theta_2, \xi/\sqrt{6})$	$(0, 0, \sqrt{24}/\xi)$
{221} 24	$(\sqrt{2}, 0, 0)$	$(\sqrt{2}, 0, -3(1 + \sqrt{2}\theta_1)/\xi)$
	$(0, \sqrt{18}, 0)$	$(0, \sqrt{2}/3, -(13/3 + \sqrt{2}\theta_2)/\xi)$
	$(1/\sqrt{2} + \theta_1, 13/\sqrt{18} + \theta_2, \xi/3)$	$(0, 0, 6/\xi)$
{311} 24	$(\sqrt{2}, 0, 0)$	$(\sqrt{2}, -\sqrt{2}/11, -(3/\sqrt{11} + \sqrt{11}/2 \theta_1 - \theta_2/\sqrt{2})/\xi)$
	$(1/\sqrt{2}, \sqrt{11}/2, 0)$	$(0, \sqrt{8}/11, -(5/\sqrt{11} + \sqrt{2}\theta_2)/\xi)$
	$(1/\sqrt{2} + \theta_1, 5/\sqrt{22} + \theta_2, 2\xi/\sqrt{11})$	$(0, 0, \sqrt{11}/\xi)$
{331} 24	$(\sqrt{2}, 0, 0)$	$(\sqrt{2}, -\sqrt{2}/19, (6/\sqrt{19} - \sqrt{19}/2 \theta_1 + \theta_2/\sqrt{2})/\xi)$
	$(1/\sqrt{2}, \sqrt{19}/2, 0)$	$(0, \sqrt{8}/19, -(12/\sqrt{19} + \sqrt{2}\theta_2)/\xi)$
	$(\theta_1, \sqrt{72}/19 + \theta_2, 2\xi/\sqrt{19})$	$(0, 0, \sqrt{19}/\xi)$
{421} 48	$(\sqrt{20}, 0, 0)$	$(1/\sqrt{5}, -\sqrt{3}/35, -\sqrt{21}(5/7 + \theta_1/\sqrt{5} - \sqrt{3}/35 \theta_2)/\xi)$
	$(3/\sqrt{5}, \sqrt{21}/5, 0)$	$(0, \sqrt{20}/21, -2(17/\sqrt{21} + \sqrt{5}\theta_2)/\xi)$
	$(6/\sqrt{5} + \theta_1, 17/\sqrt{105} + \theta_2, \xi/\sqrt{21})$	$(0, 0, \sqrt{84}/\xi)$
{321} 48	$(\sqrt{20}, 0, 0)$	$(1/\sqrt{5}, -\sqrt{18}/35, -\sqrt{14}(6/7 + \theta_1/\sqrt{5} - \sqrt{18}/35 \theta_2)/\xi)$
	$(6/\sqrt{5}, \sqrt{14}/5, 0)$	$(0, \sqrt{10}/7, -\sqrt{2}(11/\sqrt{7} + \sqrt{10}\theta_2)/\xi)$
	$(9/\sqrt{5} + \theta_1, 11/\sqrt{70} + \theta_2, \xi/\sqrt{14})$	$(0, 0, \sqrt{56}/\xi)$
{431} 48	$(\sqrt{10}, 0, 0)$	$(\sqrt{2}/5, -2/\sqrt{65}, -\sqrt{26}(19/13 + \sqrt{2}/5 \theta_1 - 2\theta_2/\sqrt{65})/\xi)$
	$(\sqrt{8}/5, \sqrt{52}/5, 0)$	$(0, \sqrt{5}/13, -\sqrt{2}(11/\sqrt{13} + \sqrt{5}\theta_2)/\xi)$
	$(9/\sqrt{10} + \theta_1, 11/\sqrt{65} + \theta_2, \xi/\sqrt{26})$	$(0, 0, \sqrt{104}/\xi)$
{432} 48	$(\sqrt{52}, 0, 0)$	$(1/\sqrt{13}, -19/\sqrt{13} \cdot 29, -\sqrt{29}(17/29 + \theta_1/\sqrt{13} - 19\theta_2/\sqrt{13} \cdot 29)/\xi)$
	$(19/\sqrt{13}, \sqrt{29}/13, 0)$	$(0, \sqrt{52}/29, -2(25/\sqrt{29} + \sqrt{13}\theta_2)/\xi)$
	$(24/\sqrt{13} + \theta_1, 25/\sqrt{13} \cdot 29 + \theta_2, \xi/\sqrt{29})$	$(0, 0, \sqrt{116}/\xi)$
{322} 24	$(\sqrt{2}, 0, 0)$	$(\sqrt{2}, 0, -\sqrt{17}(1 + \sqrt{2}\theta_1)/\xi)$
	$(0, \sqrt{34}, 0)$	$(0, \sqrt{2}/17, -\sqrt{2}(7/\sqrt{34} + \theta_2)/\xi)$
	$(1/\sqrt{2} + \theta_1, 7/\sqrt{34} + \theta_2, \xi/\sqrt{17})$	$(0, 0, \sqrt{68}/\xi)$
{332} 24	$(\sqrt{2}, 0, 0)$	$(\sqrt{2}, 0, -\sqrt{22}(1 + \sqrt{2}\theta_1)/\xi)$
	$(0, \sqrt{44}, 0)$	$(0, 1/\sqrt{11}, -\sqrt{2}(18/\sqrt{11} + \theta_2)/\xi)$
	$(1/\sqrt{2} + \theta_1, 18/\sqrt{11} + \theta_2, \xi/\sqrt{22})$	$(0, 0, \sqrt{88}/\xi)$
{410} 24	$(\sqrt{68}, 0, 0)$	$(1/\sqrt{17}, -1, -(13/\sqrt{17} + \theta_1 - \sqrt{17}\theta_2)/\xi)$
	$(\sqrt{17}, 1, 0)$	$(0, 2, -\sqrt{68}\theta_2/\xi)$
	$(13/\sqrt{17} + \theta_1, \theta_2, \xi/\sqrt{17})$	$(0, 0, \sqrt{68}/\xi)$
{430} 24	$(10, 0, 0)$	$(1/5, -1, -(7/5 + \theta_1 - 5\theta_2)/\xi)$
	$(5, 1, 0)$	$(0, 2, -10\theta_2/\xi)$
	$(7/5 + \theta_1, \theta_2, \xi/5)$	$(0, 0, 10/\xi)$
{411} 24	$(\sqrt{2}, 0, 0)$	$(\sqrt{2}, 0, -\sqrt{18}(1 + \sqrt{2}\theta_1)/\xi)$
	$(0, 6, 0)$	$(0, 1/3, -\sqrt{2}(7/3 + \theta_2)/\xi)$
	$(1/\sqrt{2} + \theta_1, 7/3 + \theta_2, \xi/\sqrt{18})$	$(0, 0, \sqrt{72}/\xi)$
{441} 24	$(\sqrt{2}, 0, 0)$	$(\sqrt{2}, 0, -\sqrt{33}(1 + \sqrt{2}\theta_1)/\xi)$
	$(0, \sqrt{66}, 0)$	$(0, \sqrt{2}/33, -\sqrt{2}(41/\sqrt{66} + \theta_2)/\xi)$
	$(1/\sqrt{2} + \theta_1, 41/\sqrt{66} + \theta_2, \xi/\sqrt{33})$	$(0, 0, \sqrt{132}/\xi)$
{433} 24	$(\sqrt{2}, 0, 0)$	$(\sqrt{2}, 0, -\sqrt{34}(1 + \sqrt{2}\theta_1)/\xi)$
	$(0, \sqrt{68}, 0)$	$(0, 1/\sqrt{17}, -\sqrt{2}(5/\sqrt{17} + \theta_2)/\xi)$
	$(1/\sqrt{2} + \theta_1, 5/\sqrt{17} + \theta_2, \xi/\sqrt{34})$	$(0, 0, \sqrt{136}/\xi)$
{443} 24	$(\sqrt{2}, 0, 0)$	$(\sqrt{2}, 0, -\sqrt{41}(1 + \sqrt{2}\theta_1)/\xi)$
	$(0, \sqrt{82}, 0)$	$(0, \sqrt{2}/41, -\sqrt{2}(71/\sqrt{82} + \theta_2)/\xi)$
	$(1/\sqrt{2} + \theta_1, 71/\sqrt{82} + \theta_2, \xi/\sqrt{41})$	$(0, 0, \sqrt{164}/\xi)$

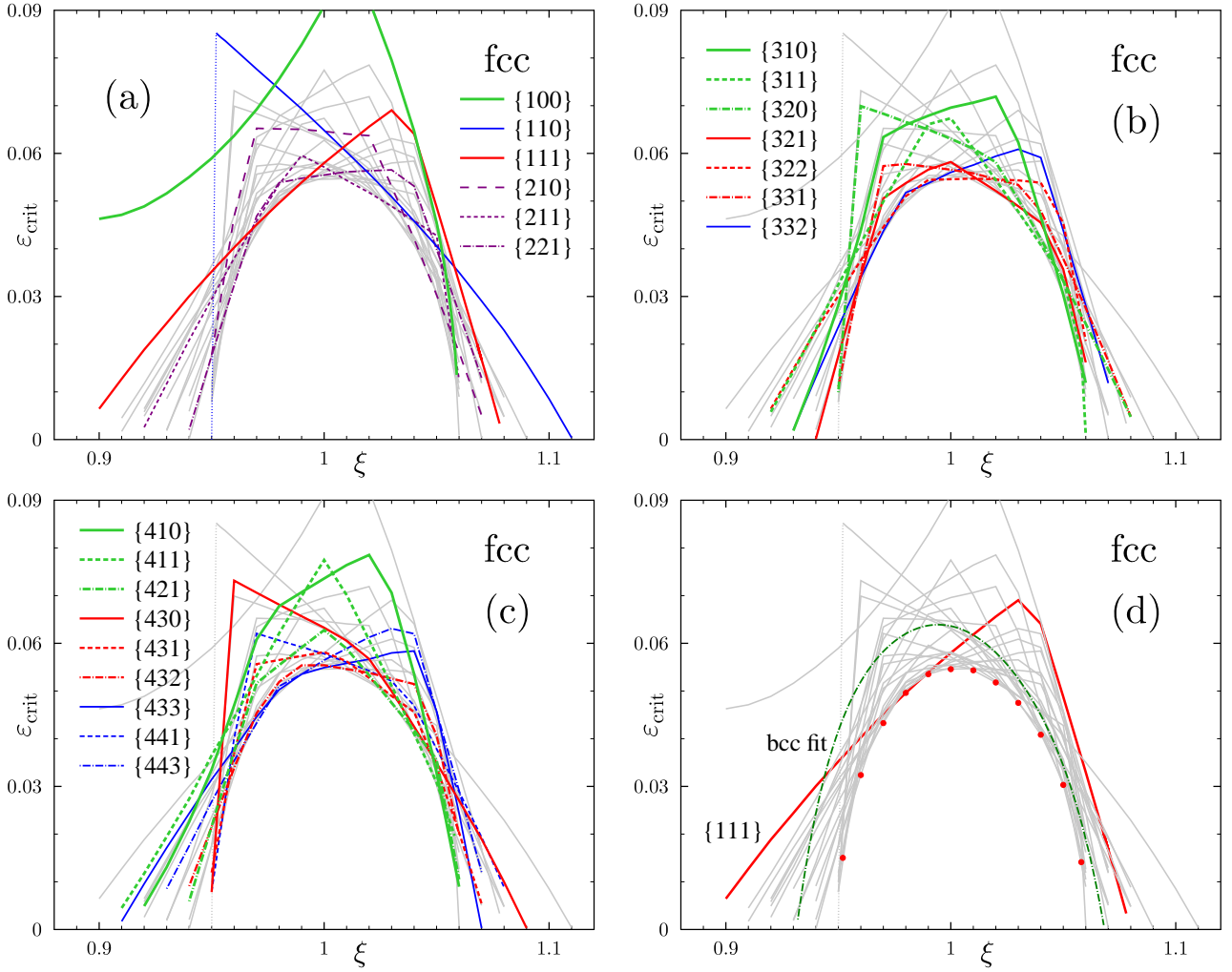


Figure 1. Breaking shear strain of stretched fc lattice for 22 crystallographic shear planes with Miller indices ≤ 4 . All panels: light-grey lines show results for all planes. (a–c) Curves of various colours, types, and thicknesses display breaking shear strain for specific planes listed in the legends. (d) Dots show present $\varepsilon_{\text{crit}}^{\text{min}}(\xi)$, dot-dashed curve is the fit of $\varepsilon_{\text{crit}}^{\text{min}}(\xi)$ from Paper I for stretched bc lattice, solid red curve reproduces $\varepsilon_{\text{crit}}(\xi)$ for growth orthogonal to the $\{111\}$ planes from panel a.

shows $\varepsilon_{\text{crit}}(\xi)$ for stretched fc lattice, growing perpendicular to a $\{111\}$ plane. These are the close-packed planes of the fcc lattice. Consequently, they are the slowest growing and they should, according to Bravais’s rule, represent the crystallization front in equilibrium (see Paper I for details). Let us reiterate that this idea is supported by the prominence of $\{111\}$ growth in terrestrial experiments on various fcc materials. In the case of near-equilibrium bottom-up crystallization in a NS crust or a WD core, we expect this type of growth in the *macrocrystallite* scenario (Paper I). Then the red curve rather than the minimum curve would determine the strength of the crystallized matter.

The data for the red curve are given in the fourth column of Table 2. To rms fit accuracy better than 0.01%, the data can be analytically approximated as:

$$\varepsilon_{\text{crit}}^{\{111\}} = \begin{cases} 0.157 - 0.099 \xi^{-4}, & \xi < 1.0355 \\ 0.4572 - 0.336 \xi^4, & \xi > 1.0355 \end{cases} \quad (2)$$

3.2 Shear modulus

If a shear deformation is not large enough to break a crystal, it may manifest itself as a transverse shear oscillation, which belongs to a class of stellar seismic modes. To describe dynamics of such modes, one needs an expression for their potential energy, which is the crystal electrostatic energy. For weak modes, the latter is a quadratic function of the strain tensor. On the other hand, we can calculate the electrostatic energy increment for an infinitesimal shear of a stretched crystal, δU , with the aid of the lattice vectors from Table 1. Identifying further $(\delta U)/V = 2\mu u_{\theta\eta}^2$, where V is the volume, we see that the quadratic dependence can be specified by an elastic coefficient μ , which can be thus determined for any stretch direction, at any ξ , and for any azimuthal angle of the shear.

Dependence of μ on the azimuthal angle turns out to be weak and, besides, there do not seem to be any arguments in favor of a particular azimuthal shear direction. Thus we shall average μ over the azimuthal angle. This yields the effective shear modulus μ_{eff} , which becomes a function of

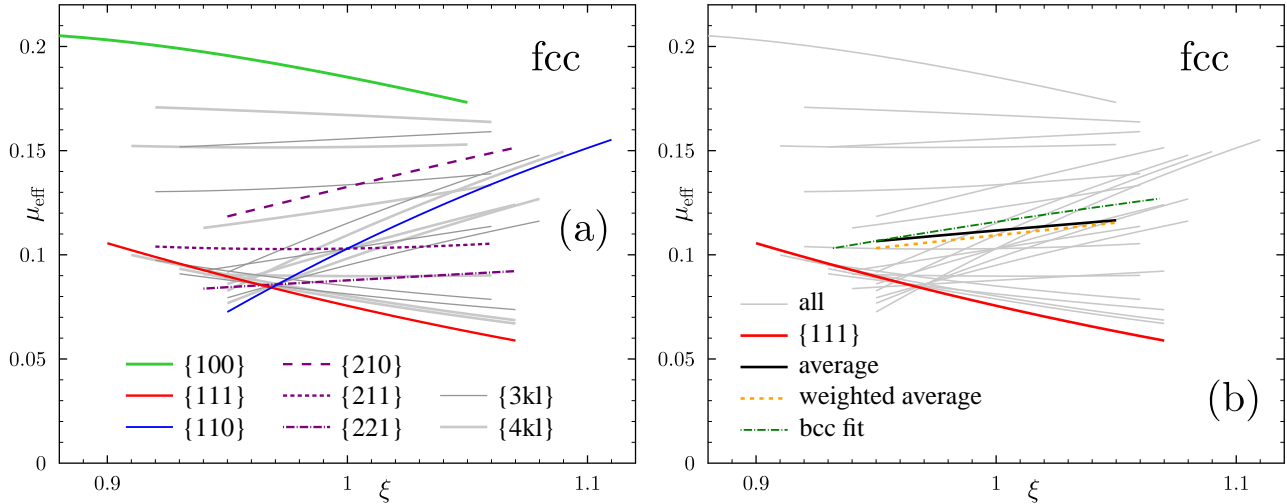


Figure 2. Effective shear moduli of stretched fcc lattice vs. stretch factor. (a) All considered shear planes. (b) All considered shear planes (solid light-grey), $\{111\}$ planes (solid red), simple-average shear modulus (solid black), weighted average shear modulus (dashed orange), simple-average shear modulus of stretched bc lattice (fit from Paper I, dot-dashed darkgreen).

Table 2. Breaking strain. Columns 1, 2, 3, and 4 show stretch factor, minimized breaking shear strain, Miller indices of the plane in which the minimum is achieved, and breaking shear strain for $\{111\}$ planes, respectively.

ξ	$\varepsilon_{\text{crit}}^{\text{min}}$	Miller index	$\varepsilon_{\text{crit}}^{\{111\}}$
0.9			0.0065
0.91			0.0127
0.92			0.0188
0.93			0.0244
0.94			0.0300
0.95			0.0352
0.952	0.0150	{441}	
0.96	0.0324	{221}	0.0403
0.97	0.0433	{443}	0.0451
0.98	0.0496	{111}	0.0496
0.99	0.0535	{443}	0.0539
1	0.0546	{322}	0.0580
1.01	0.0543	{211}	0.0618
1.02	0.0518	{211}	0.0656
1.03	0.0475	{421}	0.0690
1.04	0.0408	{311}	0.0641
1.05	0.0303	{210}	0.0488
1.058	0.0141	{410}	
1.06			0.0330
1.07			0.0168
1.072			0.0135
1.074			0.0101
1.076			0.0067
1.078			0.0034

the growth direction and the stretch factor. The quantity $\mu_{\text{eff}}(\xi)$ is shown in Fig. 2a for growth perpendicular to all 22 planes considered. Thick (green), thin (blue), and intermediate (red) solid curves correspond to the same high-symmetry planes as in Fig. 1a; long-dashed, short-dashed, and dot-dashed purple curves correspond to the same planes with the maximum Miller index of 2 as in Fig. 1a; thin dark-grey and thick light-grey lines display the shear moduli for growth perpendicular to planes with the maximum Miller index of 3 and 4, respectively.

Finally, assuming the *polycrystalline* model, i.e. the presence at a given depth of crystallites stretched vertically by the same factor but oriented in all possible ways, we average the effective shear modulus over growth orientations. The result is plotted in Fig. 2b. The family of grey curves shows shear moduli for all 22 planes, the same as in panel 2a. As in Paper I, we apply two types of averaging. For solid (black) curve, a simple averaging over 22 planes is performed (this result is denoted below as $\mu_{\text{eff}}^{\text{av}}$). Dashed (orange) curve is obtained by weighted averaging where the weights are the numbers of equivalent planes, N_{eqv} , given in the first column of Table 1. Both types of averaging produce very similar curves. The same effect was observed in Paper I for the bc lattice. The fit for simple-averaged shear modulus of the bc lattice from Paper I (equation 20) is reproduced here by dot-dashed (dark-green) line for comparison. Solid (red) curve is the effective shear modulus, $\mu_{\text{eff}}^{\{111\}}$, for crystallites growing orthogonal to $\{111\}$ planes, which plausibly should be used in the *macrocrystallite* model. To facilitate further usage, we have fitted $\mu_{\text{eff}}^{\text{av}}(\xi)$ and $\mu_{\text{eff}}^{\{111\}}(\xi)$ for the fcc lattice (to rms fit accuracy better than 0.01%) by analytic formulae:

$$\mu_{\text{eff}}^{\text{av}} = -0.18835 + 0.3\xi^{1/3}, \quad (3)$$

$$\mu_{\text{eff}}^{\{111\}} = 0.28857 - 0.713\xi^{-1/3} + 0.5\xi^{-1}. \quad (4)$$

4 DISCUSSION

The results for breaking shear strain for the fcc lattice are very similar to those for the bc lattice obtained in Paper I. Shear deformations in different planes are characterized by significantly different breaking properties. A common property for all planes (except for $\{100\}$ planes) is a reduction of breaking shear strain with deviation of the stretch factor from 1 and especially with its approach to the breaking limit for stretch. Just like in the case of the bc lattice, the $\varepsilon_{\text{crit}}^{\text{min}}(\xi)$ curve in the *polycrystalline* model is essentially parabolic. The locus of breaking strain minima of the fcc lattice lies

systematically below that for the bc structure. We do not think that this is related to the fact that fewer stretch orientations have been analyzed in Paper I.

For the unstretched fcc lattice, $\varepsilon_{\text{crit}}^{\text{min}}(1) \approx 0.055$ (to be compared with ≈ 0.064 for bcc). If we artificially reduce this number by $\sim 25\%$ to account for lattice imperfections (following Horowitz & Kadau 2009), we obtain ~ 0.04 (~ 0.05 for bcc). Breaking stretch factor for the fc lattice is found as $\xi_{\text{crit}} \approx 0.95$ and 1.06 for contractions and elongations, respectively. For breaking stretch strain, we obtain, respectively, $\tilde{\varepsilon}_{\text{crit}} \approx -0.034$ and 0.04 . This can be compared with $|\tilde{\varepsilon}_{\text{crit}}| \approx 0.04$ reported for the bc lattice by Baiko & Chugunov (2018).

In the case of near-equilibrium bottom-up crystallization in a NS crust or a WD core, we expect growth of fc crystals perpendicular to $\{111\}$ planes in the *macrocrystallite* model. Then the red curve in Fig. 1d rather than the minimum curve would determine the strength of the crystallized matter. Per equation 15 of Paper I (for NS crust), we see that the critical elongation at the mass density of, for instance, 10^9 g/cc will be achieved for ~ 1 m tall crystallites. Since the rightmost segment of the red curve is almost linear between $\xi \approx 1.04$ and $\xi_{\text{crit}} \approx 1.08$, there will be an ~ 5 cm thick layer with breaking shear strain ~ 10 times smaller than for the bulk of the crystallite and an ~ 5 mm thick layer with ~ 100 times smaller breaking shear strain. This can be easily rescaled to other mass densities with the key takeaway that $\sim 5\%$ ($\sim 0.5\%$) of crystallite height is occupied by layers one (two) orders of magnitude weaker than the bulk.

For the fc lattice, variation of the effective shear modulus with ξ and with the stretch orientation (i.e. from one shear plane to another) is not as strong as for the bc lattice (cf. figure 4 in Paper I). On the other hand, the averaged over stretch directions shear moduli are very similar between the two structures. Both types of averaging, simple and weighted, produce very similar curves. The same effect was observed in Paper I for the bc lattice.

5 CONCLUSION

It has been argued in Paper I that unidirectional near-equilibrium freezing of dense matter in compact stars (from the deeper layers outward) preserves the microscopic order of previously crystallized layers and is accompanied by gradual vertical stretching of crystal elementary cells in response to pressure and electron density reduction. Overstretched crystals break, which limits the vertical sizes of growing crystallites. In Paper I, elastic and breaking properties of such matter have been analyzed under the assumption of bc lattice structure. In this work, the analysis has been extended to fc configurations. In particular, we have studied shear deformations of stretched fc crystals in planes orthogonal to the stretch direction. We have considered shear in all 22 crystallographic planes characterized by Miller indices ≤ 4 . This should be contrasted with the analysis in Paper I, where only 7 planes (3 of the highest symmetry and 4 less symmetric) have been studied.

Our conclusions are very similar to those of Paper I. In particular, a common property for all planes is a reduction of breaking shear strain with deviation of the stretch

factor from 1 and especially with its approach to the breaking limit for stretch. Shear deformations in different planes are characterized by significantly different breaking properties. Assuming the *polycrystalline* model of matter, the breaking shear strain at each stretch factor ξ has been minimized over stretch directions. Similar to the bc configuration, the locus of these minima was found to be essentially parabolic. At $\xi = 1$, the minimum breaking shear parameter $\varepsilon_{\text{crit}}^{\text{min}}(1) \approx 0.055$ (to be compared with ≈ 0.064 for bcc). The $\varepsilon_{\text{crit}}^{\text{min}}(\xi)$ curve for the fc structure lies systematically below that for the bc structure. We do not think that this is related to the fact that fewer stretch orientations have been analyzed in Paper I. In both cases, for certain ξ , the minima are achieved for low-index planes. For convenience, the $\varepsilon_{\text{crit}}^{\text{min}}(\xi)$ curve for the fc lattice has been fitted by a simple analytic expression.

We have also determined the effective shear moduli vs. the stretch factor for shear deformations perpendicular to the stretch direction for all 22 shear planes. For the fc lattice, the variation of these curves with ξ and from one shear plane to another is not as strong as for the bc lattice (cf. figure 4 in Paper I). On the other hand, the averaged over stretch orientations shear moduli are very similar between the two structures.

It is possible that the epitaxial crystallization in compact star matter results in a formation of large-scale crystallites. Optionally, it seems plausible that, in agreement with the Bravais's rule, the entire crystallization front grows orthogonal to the close-packed planes, which, for the fc structure, are the $\{111\}$ planes (see Paper I for discussion). In this *macrocrystallite* scenario, peculiar properties of ideal crystals oriented in a certain way may manifest themselves in astrophysical phenomena. For instance, if we assume the fc lattice growth perpendicular to the $\{111\}$ planes, we expect the appearance of layers with the thickness of $\sim 5\%$ ($\sim 0.5\%$) of the crystallite height whose breaking shear strain is 10 (100) times lower than for the bulk of the crystallite. Such structure of stellar matter may help explain rich observational phenomenology of magnetars with active episodes accompanied by numerous bursts and outbursts.

REFERENCES

- Carini P., Kalman G., Golden K. I., 1982, Phys. Rev. A, 26, 1686
- Kalman G., Golden K. I., 1990, Phys. Rev. A, 41, 5516
- Golden K. I., Kalman G., Wyns P., 1992, Phys. Rev. A, 46, 3454
- Golden K. I., Kalman G. J., 2000, Physics of Plasmas, 7, 14
- Donkó Z., Kalman G. J., Golden K. I., 2002, Phys. Rev. Lett., 88, 225001
- Haensel P., Potekhin A. Y., Yakovlev D. G., 2007, Neutron Stars 1: Equation of State and Structure. Springer, New York
- Van Horn H. M., 1968, ApJ, 151, 227
- Hansen J.-P., McDonald I. R., Pollock E. L., 1975, Phys. Rev. A, 11, 1025
- Ott T., Baiko D. A., Kählert H., Bonitz M., 2013, Phys. Rev. E, 87, 043102
- Kaspi V. M., Beloborodov A. M., 2017, ARA&A, 55, 261

- Ushomirsky G., Cutler C., Bildsten L., 2000, MNRAS, 319, 902
Baiko D. A., 2024, MNRAS, 528, 408 (Paper I)
Baiko D. A., Kozhberov A. A., 2017, MNRAS, 470, 517
Baiko D. A., Chugunov A. I., 2018, MNRAS, 480, 5511
Horowitz C. J., Kadau K., 2009, Phys. Rev. Lett., 102, 191102